

Possibility to study η -mesic nuclei and photoproduction of slow η -mesons at the GRAAL facility

V.A. Baskov¹, J.P. Bocquet², V. Kouznetsov³, A. Lleres², A.I. L'vov¹,
L.N. Pavlyuchenko¹, V.V. Polyanski¹, D. Rebrevend², G.A. Sokol^{1,*}

¹*P.N. Lebedev Physical Institute, Leninsky prospect 53, 119991 Moscow, Russia*

²*Laboratoire de Physique Subatomique et de Cosmologie,
53, av. des Martyrs, F-38026 Grenoble Cedex, France*

³*Institute for Nuclear Research, 60-th October Anniversary prospect 7a, 117312 Moscow, Russia*

A new experiment is proposed with the aim to study η -mesic nuclei (bound systems of the η -meson and a nucleus) and low-energy interactions of η with nuclei. Two decay modes of η produced by a photon beam in the subprocess $p(\gamma, p_1)\eta$ on a proton p inside the nucleus A will be observed, namely a collisional decay $\eta N \rightarrow \pi N$ inside the nucleus and the radiative decay $\eta \rightarrow \gamma\gamma$ outside. In addition, a collisional decay of stopped $S_{11}(1535)$ resonance inside the nucleus, $S_{11}(1535)N \rightarrow NN$, will be studied. Triggers of the corresponding reactions are triple ($\pi^0 pp_1$), ($\gamma\gamma p_1$), or ($p_1 p_2 p_3$) coincidences which include two particles from the η or $S_{11}(1535)$ decays and a nucleon p_1 flying forward in the case when a slow η is produced.

η -nuclei are expected to be observed as peaks in the energy distribution of πN or NN pairs. This will bring an information on binding energies and widths of η -nuclei, as well as an information on $S_{11}(1535)$ -nucleus interactions at subthreshold energies of η . Studies of slow- η production through the radiative decay mode will give an information on η -nucleus interaction at energies above threshold of η production.

The experiment can be performed using the tagged photon beam at ESRF with the end-point energy $E_{\gamma \max} \approx 1000$ MeV and the GRAAL detector which includes a high-resolution BGO calorimeter and a large acceptance lead-scintillator time-of-flight wall. Some results of simulation and estimates of yields are given.

* E-mail: gsokol@x4u.lebedev.ru

Contents

I. Introduction: ηN interaction and η-nuclei	3
A. Sources of information	3
B. Eta-mesic nuclei	4
C. Hunting η -mesic nuclei: negative results	6
D. Hunting η -mesic nuclei: positive results from photoproduction	6
II. Layout of a new experiment	8
A. The experimental setup and scenarios of measurements	8
B. Monte-Carlo simulation of the detection of πN and NN events	11
C. Estimates of count rates	15
III. Summary of aims and perspectives	17
Acknowledgments	19
References	19

I. INTRODUCTION: ηN INTERACTION AND η -NUCLEI

A. Sources of information

Interaction of η mesons with other hadrons including nucleons and nuclei is not yet well understood. Being a member of the $SU(3)$ octet of pseudoscalar mesons, η has a spatial structure similar to that of the pion. However, η has isospin 0 and contains about 50% of strange quarks ($s\bar{s}$). It is much heavier than the pion (547 MeV versus 140 MeV). Moreover, η (and especially η') is strongly mixed with gluons which contribute through the $U_A(1)$ anomaly and make η' heavier than η . For all these reasons, chiral symmetry which underlies pion dynamics at low energies put far less constraints onto the low-energy dynamics of η .

Nowadays, it is generally assumed that ηN interaction at low energies is dominated by production and decay of the intermediate $S_{11}(1535)$ resonance ($J^P = \frac{1}{2}^-$) which overlaps ηN threshold ($m_\eta + m_N = 1486$ MeV) within the total width of the resonance, $\Gamma[S_{11}(1535)] \simeq 150$ MeV. Most of experimental information on the ηN interaction comes from studies of the reactions $\pi^- p \rightarrow \eta n$ and $\gamma N \rightarrow \eta N$ followed by their comparison with similar processes, in which η is replaced by the pion (i.e. $\pi N \rightarrow \pi N$ and $\gamma N \rightarrow \pi N$). Such a comparison is not straightforward and subject to model uncertainties.

Assuming the $S_{11}(1535)$ dominance, the s -wave Breit-Wigner cross sections of the above reactions are proportional to partial widths of the $S_{11}(1535)$ resonance:

$$\begin{aligned}\sigma(\pi N \rightarrow \pi N) &\sim \Gamma_\pi \Gamma_\pi, \\ \sigma(\pi N \rightarrow \eta N) &\sim \Gamma_\pi \Gamma_\eta, \\ \sigma(\gamma N \rightarrow \pi N) &\sim \Gamma_\gamma \Gamma_\pi, \\ \sigma(\gamma N \rightarrow \eta N) &\sim \Gamma_\gamma \Gamma_\eta.\end{aligned}\tag{1}$$

From the first two channels, the π - and η -widths and couplings of $S_{11}(1535)$ can be found. Furthermore, the cross section of ηN scattering can be derived too via

$$\sigma(\eta N \rightarrow \eta N) \sim \Gamma_\eta \Gamma_\eta.\tag{2}$$

Following this line in a modified form (in the framework of the couple-channel formalism), Bhalerao and Liu [1] estimated the ηN scattering amplitude and found, in particular, the ηN scattering length

$$a_{\eta N} = (0.27 + i 0.22) \text{ fm}.\tag{3}$$

Using the third channel in (1), the radiative width of $S_{11}(1535)$ can also be determined. A result obtained by the VPI-GWU group [2] and based on their partial-wave analysis of pion photoproduction (SAID) reads $A_{1/2}^p \simeq 0.060$ GeV $^{-1/2}$ (for the proton target) and $A_{1/2}^n \simeq -0.020$ GeV $^{-1/2}$ (for the neutron one) in terms of the photocouplings $A_{1/2} \sim \sqrt{\Gamma_\gamma}$. Alternatively, the same radiative widths and photocouplings can be determined from the fourth channel in (1). Using Mainz data on η photoproduction off protons and deuterons, the result was obtained [3, 4] which was dramatically different from the previous findings: $A_{1/2}^p \simeq 0.110$ GeV $^{-1/2}$ and $A_{1/2}^n \simeq -0.8A_{1/2}^p$. Thus, the radiative decay width of $S_{11}^+(1535)$, being determined through π -photoproduction, is by the factor of ~ 4 less than the one determined through η -photoproduction. This difference is even larger in the case of $S_{11}^0(1535)$.

Such a large discrepancy implies that the factorization of the cross sections cannot be valid and therefore large nonresonance backgrounds persist in some, if not all, considered

channels. In Ref. [5], a dynamical model was developed, in which nonresonance backgrounds were explicitly evaluated and indeed found to be very essential and large. It is often claimed that the radiative widths of $S_{11}(1535)$ must be determined through η photoproduction, where the background is allegedly small, and must not be determined through π one, where the background may be larger due to influence of a few overlapping resonances. In particular, in a recent update of the SAID analysis of pion photoproduction [6] the photocouplings of the $S_{11}(1535)$ resonance are announced to be "too uncertain to be quoted". Even so, our knowledge of ηN couplings and interactions crucially depends on the factorization and extrapolation which leads us from experimentally investigated channels (1) to the unknown one, ηN scattering (2).

In modern phenomenological analyses specific assumptions made on resonances and backgrounds are different from those assumed in [1]. In particular, more high-lying resonances are included, what is effectively equivalent to considering the background in the older approach energy dependent. These changes, being physically marginal, have however a great impact on the derived ηN scattering amplitude. For example, the ηN scattering length found in recent works through a coupled-channel analysis of the first two reactions in (1) reads

$$\begin{aligned} a_{\eta N} &= (0.75 \pm 0.04) + i(0.27 \pm 0.03) \text{ fm} & [7], \\ a_{\eta N} &= (0.717 \pm 0.030) + i(0.263 \pm 0.025) \text{ fm} & [8]. \end{aligned} \quad (4)$$

Note a dramatic difference in the real part of $a_{\eta N}$.

With more channels included and with the background structure more complicated, the result for $a_{\eta N}$ may change again. Currently, phenomenological analyses ignore channels involving strange particles ($\pi N \rightarrow K\Lambda$, $\pi N \rightarrow K\Sigma$, $\eta N \rightarrow K\Lambda$, and $\eta N \rightarrow K\Sigma$) — simply because of the lack of experimental data in the η sector. Meanwhile it was theoretically shown [9] that an interplay of strange channels with nonstrange ones can generate an energy-dependent structure in πN and ηN reactions which is very similar to that usually associated with the $S_{11}(1535)$ resonance. Thus, even the very dominance in the above reactions of the fundamental three-quark state, the $S_{11}(1535)$ resonance, over the dynamically generated coupled-channels peaks (hadron molecules) becomes questionable.

In order to bring new experimental constraints, to check the factorization, to test a truncated coupled-channel dynamics, and at the end to arrive at a more reliable knowledge of properties of the $S_{11}(1535)$ resonance, direct data on ηN interaction are badly needed. They can, in principle, be obtained through studies of η in the final states of nuclear reactions. This naturally suggests a need for 1) investigations of the energy region near but above ηN threshold, where ηN scattering affects cross sections through the final-state interaction, and 2) investigations of the subthreshold energy region, where formation of bound states of η and a nucleus is possible. Experimental studies of bound states of various ηA systems would greatly contribute to learning elementary ηN scattering and, more generally, to understanding of meson-baryon interactions in the second nucleon-resonance region.

B. Eta-mesic nuclei

Eta-mesic nuclei (${}_{\eta}A$) are a new kind of short-living nuclei which consist of ordinary particles, i.e. nucleons, and a lighter one, the η -meson, which is bound by nuclear forces with the nucleons. The η -nuclei have many resemblances with better-studied Λ - and Σ -hypernuclei which consist of nucleons and Λ or Σ , respectively. A big difference is, however,

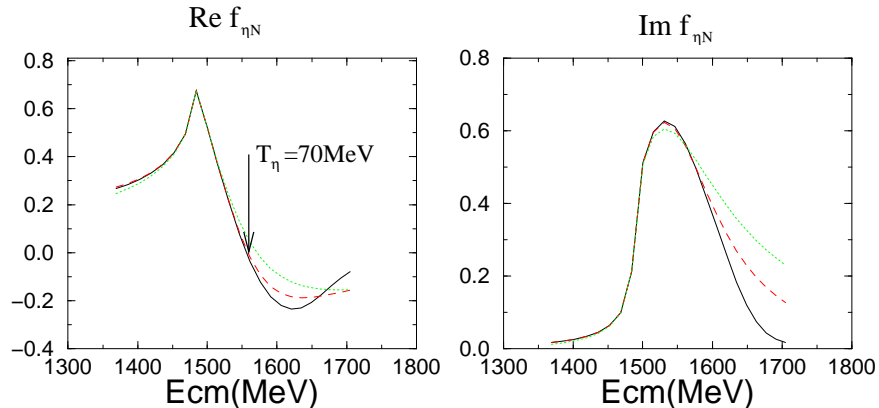


FIG. 1: Energy dependence of the ηN scattering amplitude $f_{\eta N}$ (in units of fm) [7].

in the life-time, because η -nuclei decay via strong rather than weak interaction. A typical width of bound- η levels in nuclei is of order 10–30 MeV [10–12] or even 30–50 MeV [13, 14]. Annihilation of the bound η -meson through the reaction $\eta N \rightarrow S_{11} \rightarrow \pi N$ in the nuclear matter dominates this width. About 10–20% of the width is caused by the collisional process $N S_{11}(1535) \rightarrow NN$ [15]. A tiny fraction of η -decays inside the nucleus (of order $5 \cdot 10^{-5}$) happens due to the two-photon decay $\eta \rightarrow \gamma\gamma$ too. Due to virtual transitions between ηN states and the $S_{11}(1535)$ resonance, part of time the η -nucleus is seen as a complex of $S_{11}(1535)$ and $A - 1$ nucleons.

The very existence of the bound η -A states [10, 16] is possible because the positive real part of $a_{\eta N}$ results in an average attraction between a slow η and a nuclear matter. This attraction is (roughly) characterized by the first-order optical potential

$$2m_{\eta}V_{\eta}(r) = -4\pi\rho(r)a_{\eta N}\left(1 + \frac{m_{\eta}}{m_N}\right), \quad (5)$$

where $\rho(r)$ is the nuclear density. Depending on the magnitude of the scattering length $a_{\eta N}$, such an attraction is sufficient for binding η in all nuclei of sufficient size — namely those with $A \geq 11$, if Eq. (3) is used, or even those with $A \geq 4$, if newer values of $a_{\eta N}$, Eq. (4), are valid. With slightly larger $a_{\eta N}$, η -bound states are possible for $A = 3$ and $A = 2$ too [17].

When the kinetic energy of η is not zero, the optical potential becomes proportional to the ηN scattering amplitude $f_{\eta N}$. The real part of $f_{\eta N}$, the threshold value of which is just equal to the scattering length $a_{\eta N}$, is expected to remain positive up to kinetic energies of η below 70 MeV (see Fig. 1). This means that the effective ηA attraction probably exists in a wide near-threshold energy region, $\Delta E_{\eta} \approx 0-70$ MeV.

The attractive forces in the final state must lead to a near-threshold enhancement in the total and differential cross section of real- η production by different beams. Such an enhancement was indeed observed in several reactions including $p(d, {}^3\text{He})\eta$ [18, 19], $d(d, {}^4\text{He})\eta$ [20] and ${}^2\text{H}(\gamma, \eta)$, ${}^4\text{He}(\gamma, \eta)$ [21], thus supporting the existence of a rather strong ηA attraction even for the lightest nuclei. Nevertheless, all these experiments, which have deal with η in the final state, cannot directly prove that bound ηA states do really exist. A well-known counter-example is provided by the NN system in the ${}^1\text{S}_0$ state, which has a virtual rather than real level described by a *negative* rather than positive scattering length. Therefore, direct observations of bound states through studies of the subthreshold energy region are

certainly needed in order to fully reconstruct the ηA optical potential and the elementary ηN scattering amplitude. At energies above the threshold, studies of real- η production on nuclei with different A are needed in order to investigate the optical potential at different nuclear densities. Generally, experimental studies of various ηA systems in the discrete and continuous spectrum would greatly contribute to understanding of meson-baryon interactions in the second nucleon-resonance region.

C. Hunting η -mesic nuclei: negative results

Two attempts to discover η -nuclei in the missing mass spectrum of the reaction $\pi^+ A \rightarrow pX$ were performed at Brookhaven [22] and Los Alamos [23] soon after the first theoretical suggestions [10]. It was then expected that a capture of a produced slow η to a bound level(s) would result in a peak(s) of the width ~ 10 MeV near the end of the kinetic energy spectrum of the knocked-out forward-flying protons. However, narrow peaks were found neither in [22], nor in [23].

An explanation was soon suggested in Ref. [15], in which the imaginary part of the optical ηA potential V_η was argued to get a great increase owing to the two-pion absorption of η via the reaction $\eta N \rightarrow S_{11}(1535) \rightarrow \pi\pi N$. Accordingly, a great increase in the widths of bound- η levels was predicted too. The conclusion of Ref. [15] was that the bound- η levels in nuclei may be so wide that they strongly overlap and hence a broad bump arises instead of a set of narrow lines in the spectrum. This was exactly what the experiment [23] showed, in which a broad bump of the width ≥ 30 MeV was observed approximately at the place where narrow peaks were earlier predicted [10].

There is, however, a flaw in the above explanation, because a large increase in $\text{Im } V_\eta$ is obtained in [15] only with the mass, the width and the couplings of $S_{11}(1535)$ which do not accurately reproduce available experimental data on the reaction $\pi^- p \rightarrow \eta n$. When these parameters are changed in order to fit the data, the dramatic increase of the widths completely disappears (see the second columns in the Table 1 of Ref. [15]). In a more recent work [11], the absence of huge medium effects on the imaginary part of the optical potential V_η was re-established and a physical picture with relatively narrow levels was confirmed. Very recent calculations [12–14] agree with these findings.

Still, there is another physical reason for unresolving narrow lines. The point is that the η -mesic nucleus can be produced with excited nucleon degrees of freedom. That is, the energy of the nuclear core which binds η is not fixed but rather smeared over the Fermi sea. Such a Fermi smearing also contributes to broadening peaks in the observed spectra and makes it more difficult to disentangle them from a smooth background.

The conclusion is that the negative results [22, 23] of a search for η -mesic nuclei in the previous missing-mass experiments do not necessary mean that such physical objects either do not exist or dissolve in the continuum. Rather the inclusive method of [22, 23] was less reliable for searching for broad peaks and hence for measuring energy levels of η -mesic nuclei than it was then assumed.

D. Hunting η -mesic nuclei: positive results from photoproduction

Recently, the first positive signal for η -mesic nuclei was observed in a photoreaction [24]. In contrast to the inclusive experiments [22, 23], decay products of η -mesic nuclei have been

detected in that work. The experiment was performed at the bremsstrahlung photon beam of the 1 GeV electron synchrotron of Lebedev Institute. The reaction studied was

$$\gamma + {}^{12}\text{C} \rightarrow p(n) + {}^{11}_{\eta}\text{B} ({}^{11}_{\eta}\text{C}) \rightarrow p(n) + \pi^+ + n + X = \pi^+ + n + X'. \quad (6)$$

A slow η -meson produced in the subprocess $\gamma N \rightarrow S_{11}(1535) \rightarrow \eta N$ is captured into a quasi-bound state. After some time-delay, it annihilates inside the nucleus and gives a $\pi^+ n$ pair through the subprocess $\eta p \rightarrow S_{11}^+(1535) \rightarrow \pi^+ n$ (see Fig. 2a). A fast nucleon emitted forward at the first stage of the reaction escapes the nucleus, whereas components of the $\pi^+ n$ pair fly isotropically and they are detected by scintillator time-of-flight spectrometers placed transversely to the photon beam in opposite directions.

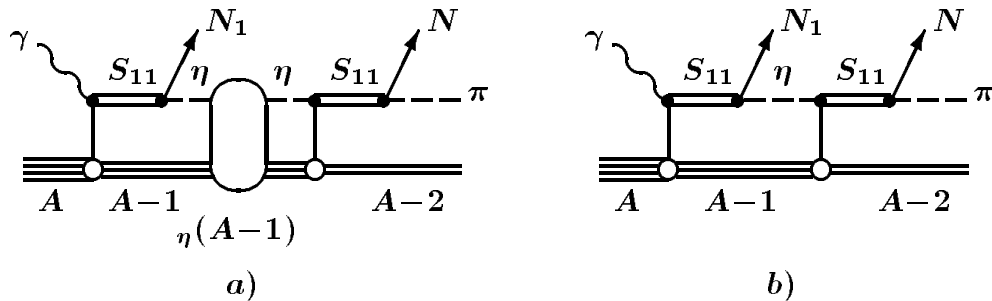


FIG. 2: a) Mechanism of formation and decay of η -nuclei in a photoreaction; b) Production of πN pairs through intermediate η in the absence of ηA attraction.

Note that transversely flying $\pi^+ n$ pairs cannot be produced via the one-step reaction $\gamma p \rightarrow \pi^+ n$ in the nucleus, whereas they naturally appear through an intermediate slow- η agent. In principle, nothing prevents the chain $\gamma N \rightarrow \eta N$, $\eta N \rightarrow \pi N$ to happen in the absence of the η -nucleus attraction V_η too (see Fig. 2b). However, theoretical estimates given in [24, 25] show that the binding effects enhance the yield of the pairs with a low total 3-momentum by the factor of ~ 100 and lead to a full dominance of the reaction mechanism related with a formation of the intermediate η -mesic nucleus in the subthreshold region of the invariant mass $\sqrt{s_{\pi^+ n}} < m_\eta + m_N$. A clear peak in the invariant-mass distribution is therefore predicted in the subthreshold region (see Fig. 3 which show so-called spectral functions representing probabilities to find an intermediate η -meson with the (kinetic) energy E and momentum q [25, 26]).

Such a peak was indeed observed in the experiment, provided the photon beam energy $E_{\gamma \max}$ exceeded the η -production threshold off the free nucleon (707 MeV). The peak was absent when $E_{\gamma \max}$ was below threshold. See Fig. 4, in which data shown are obtained by applying an unfolding procedure to raw experimental velocity-distributions found by the time-of-flight technique. The unfolding procedure used is based on the statistical method of solving the inverse problem [27].

Subtracting a smooth background, a one-dimensional distribution of the $\pi^+ n$ pairs over their total energy has also been found (Fig. 5). Its width is about 150 MeV including the experimental resolution of the setup. Its center lies by $\Delta E = 40 \pm 15$ MeV lower than ηN threshold, $m_\eta + m_N = 1486$ MeV, and by 90 MeV lower than the $S_{11}(1535)$ resonance mass. The shift in the peak position with respect to the threshold provides an evidence for seeing binding effects for η in the nucleus.

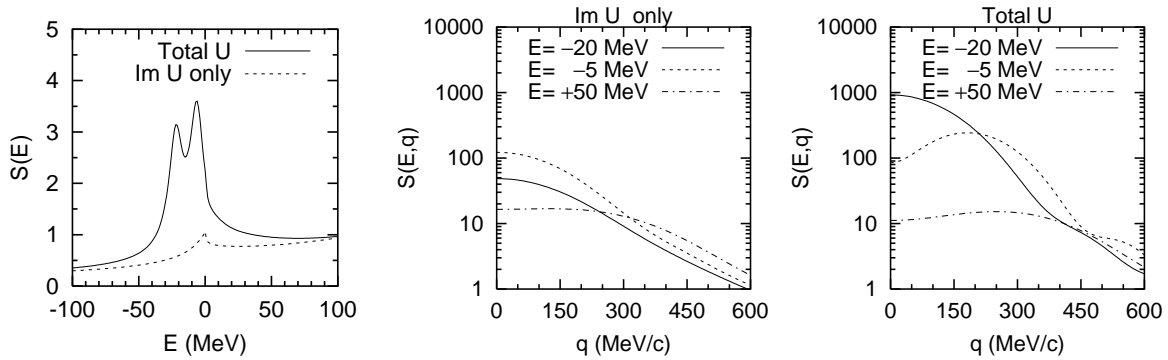


FIG. 3: Spectral functions $S(E)$ and $S(E, q)$ (in arbitrary units) found with a rectangular-well optical potential simulating the nucleus ^{12}C . For a comparison, shown also are results obtained with dropping out the attractive (i.e. real) part of the ηA potential.

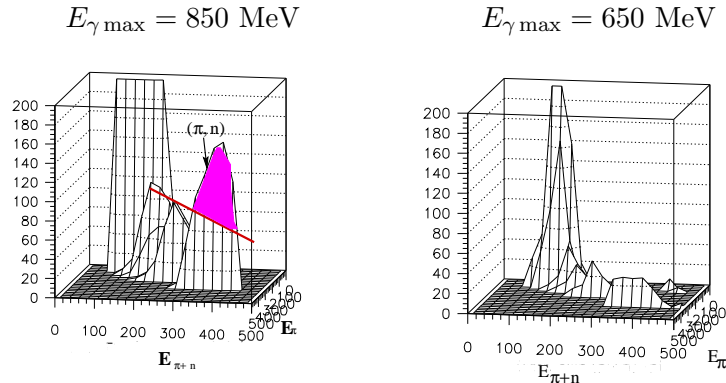


FIG. 4: Two-dimensional distributions over the total kinetic energy of the π^+n pair, E_{π^+n} , and the kinetic energy of the π^+ -meson, E_{π^+} , for two energies $E_{\gamma\text{max}}$ of the bremsstrahlung photon beam [26].

II. LAYOUT OF A NEW EXPERIMENT

A. The experimental setup and scenarios of measurements

The main aim of the proposed experiment is measuring the energy- and A -dependence of the cross section of η -mesic-nucleus photoproduction, as well as measuring the ratio of πN and NN yields which are connected with probabilities of the processes $S_{11}(1535) \rightarrow \pi + N$ and $S_{11}(1535) + N \rightarrow N + N$ inside different nuclei. Also, data on production of slow η off different nuclei will be collected with the end aim to learn the optical potential V_η in the near-threshold region. The reactions to be studied are

$$\gamma + A \rightarrow p_1 + \eta(A-1) \rightarrow p_1 + \pi^0 + p + X \rightarrow p_1 + \gamma_1 + \gamma_2 + p + X \quad (7)$$

(see Fig. 6),

$$\gamma + A \rightarrow p_1 + \eta(A-1) \rightarrow p_1 + p_2 + p_3 + X \quad (8)$$

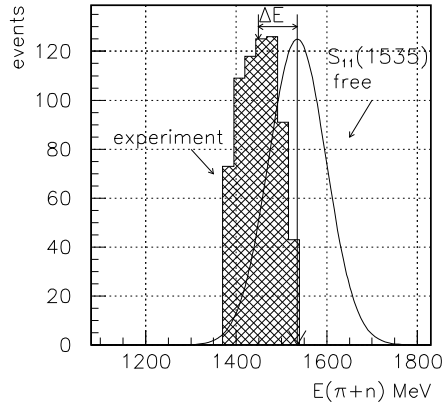


FIG. 5: Distribution over the total energy of the π^+n pair after a subtraction of the background.

(see Fig. 7), and

$$\gamma + A \rightarrow p_1 + \eta(A-1) \rightarrow p_1 + \gamma_1 + \gamma_2 + X \quad (9)$$

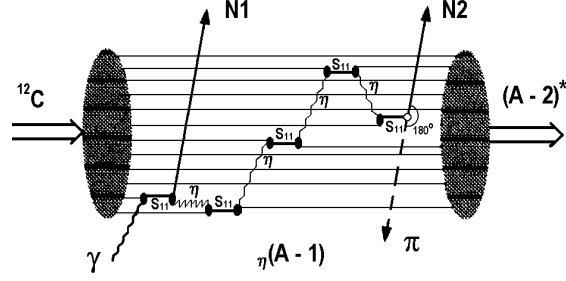
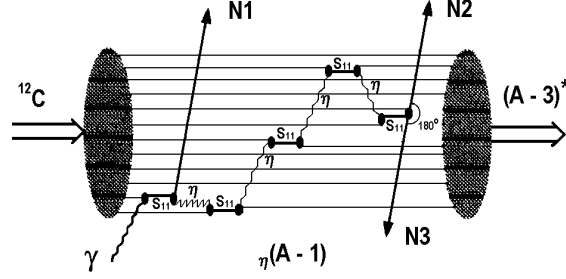
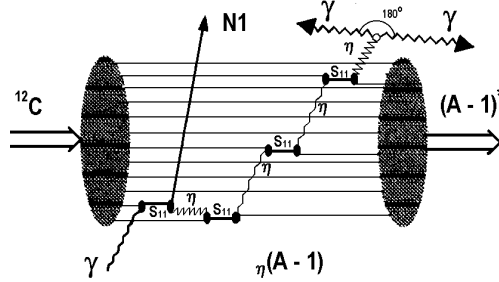
(see Fig. 8), where the proton p_1 flying forward is produced at the stage of creating a slow η -meson inside the nucleus via the subprocess $\gamma p \rightarrow \eta p_1$ (the kinematics of this subprocess in the case of p at rest is shown in Fig. 9). Depending on whether the produced η -meson annihilates electromagnetically or through the strong reaction $\eta p \rightarrow S_{11}(1535) \rightarrow \pi^0 N$, either two photons with the invariant mass of the η -meson or two photons from π^0 plus a proton flying in the opposite direction are to be detected. In the case when the $S_{11}(1535)$ resonance annihilates collisionally through the two-nucleon mode, two protons emerge which fly in opposite directions. A rough estimate for relative rates of these three outcomes (6), (7), (8) is $1 : 10^{-1} : 10^{-5}$.

In contrast to the first two cases (6) and (7), the reaction (8) directly provides, through the full energy $E(\gamma_1 + \gamma_2)$ of gammas, the energy of the η produced. Unfortunately, it is very difficult to use this energy information for determination of the binding energy of η in the nucleus because of the very low probability ($\sim 10^{-5}$) of bound η to decay through the electromagnetic mode. Moreover, owing to a limited energy resolution of photon detectors, the $\gamma\gamma$ events from the bound- η decays can be lost on the background of $\gamma\gamma$ pairs arising after photoproduction of slow η -mesons without a formation of the η -nucleus, what exactly happens at energies slightly above threshold. Nevertheless, a measurement of $E(\gamma_1 + \gamma_2)$ provides a good way for studying energy dependence of near-threshold ηA interaction.

The experiment can be performed using the tagged photon beam at ESRF with the maximum energy $E_{\gamma \max} \simeq 1000$ MeV and the GRAAL apparatus. The trigger consists of a simultaneous detection of the forward-flying proton p_1 plus two photons from π^0 or η . In addition, the presence of a fast proton p from a $\pi^0 p$ pair (decay products of $S_{11}(1535) \rightarrow \pi N$) is analyzed, as well as the presence of two protons from the reaction $S_{11}(1535) + N \rightarrow N + N$.

The GRAAL apparatus (Fig. 10) consists of a high-resolution large solid-angle electromagnetic BGO-calorimeter combined with multiwire proportional chambers (MWPC) which cover a solid-angle range of near 4π . Particles emitted at small angles are also detected by a scintillator wall which is installed three meter apart from the target; it enables particle's identification by means of their time-of-flight and their energy losses ΔE in scintillators.

The particle identification in the central region is accomplished with a plastic scintillator barrel through the measurement of dE/dx . The BGO crystals are of 8 different dimensions. They are shaped like pyramidal sectors with a trapezoidal basis. They define 15 angular

FIG. 6: Photoproduction of a η -nucleus and its decay through the πN mode.FIG. 7: Photoproduction of a η -nucleus and its decay through the NN mode.FIG. 8: Photoproduction of a slow η -meson and its decay through the $\gamma\gamma$ mode. This decay may happen both inside and (mostly) outside the nucleus.

regions in the polar angle θ (the polar axis being the symmetry axis of the calorimeter coincident with the photon-beam axis) and 32 angular regions in the azimuthal angle ϕ .

All the 480 crystals have the same length of 24 cm (i.e. > 21 radiation lengths) ensuring a good absorption of photon showers in the 1 GeV energy region. The crystals are arranged in such a way that reaction products emitted in any directions around the target center encounter a constant thickness of the BGO. More detail on the performance of the BGO calorimeter and the time-of-flight wall can be found in Refs. [28, 29]

In the experiment, the forward-flying proton p_1 will be detected by the time-of-flight wall, whereas two photons from π^0 or η decays plus protons from $\pi^0 p$ (with $E_p \sim 100$ MeV) or pp pairs (with $E_p \sim 300$ MeV) which are products of $S_{11}(1535) \rightarrow \pi N$ and $S_{11}(1535) + N \rightarrow N + N$, respectively, will be detected by the BGO calorimeter and multiwire chambers.

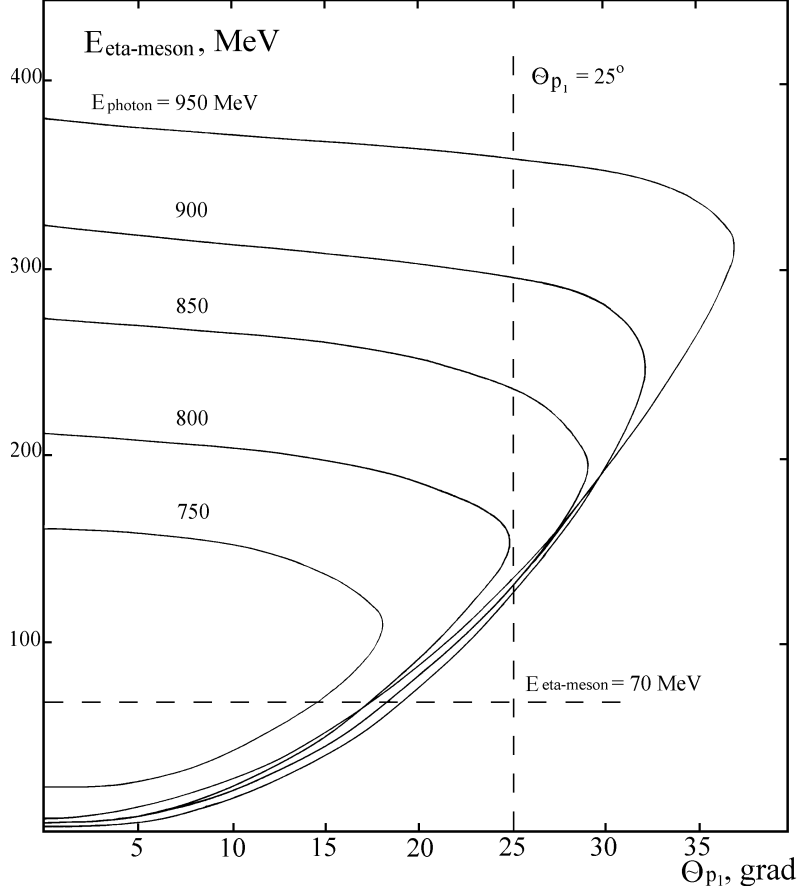


FIG. 9: Kinematics of η -meson photoproduction off the free proton, $\gamma p \rightarrow \eta p_1$.

B. Monte-Carlo simulation of the detection of πN and NN events

Since the BGO calorimeter does not ensure a sufficient accuracy in measuring energies of neutrons and charged pions, most of πN and NN channels are not suitable for the planned measurements. The exceptions are $\pi^0 p$ and pp channels. This statement is illustrated by a simple Monte-Carlo estimate using the GEANT code. 10^3 events were generated assuming a sample kinematics in which the nucleon and the π -meson fly from the center of a small $1 \text{ cm} \times 1 \text{ cm} \times 1 \text{ cm}$ ^{12}C target with the kinetic energy of 100 MeV and 300 MeV, respectively, in opposite directions and exactly transversely to the photon beam ($\theta_N = \theta_\pi = 90^\circ$). The BGO blocks were taken to have a semi-cylinder form each with the size $50 \text{ cm} \times 50 \text{ cm} \times 25 \text{ cm}$, so that the pion and the nucleon strike the centers of the BGO1 and BGO2 blocks shown in Fig. 11). Energy losses in the target and in the air between the target and the calorimeter have been taken into account.

Energy depositions in and angular distributions reconstructed through such a model BGO calorimeter are shown in Figs. 12, 13, 14 and 15 for the channels $\pi^+ n$, $\pi^- p$, $\pi^0 p$, and $\pi^0 n$, respectively. In the last two cases we also show a reconstructed direction θ_{π^0} of the π^0

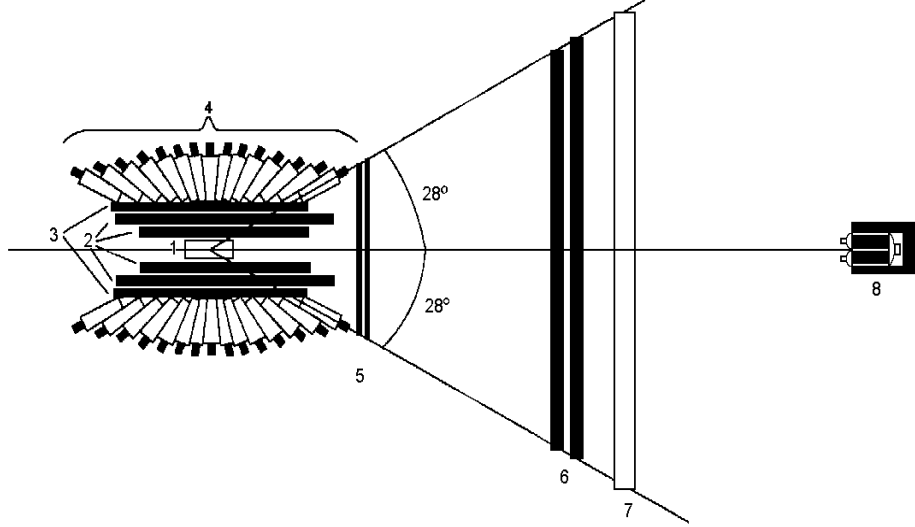


FIG. 10: Layout of the GRAAL apparatus. 1: Liquid-hydrogen target; 2: Cylindric wire chambers; 3: Plastic scintillator barrel; 4: BGO crystals; 5: Plane wire chambers; 6: Double scintillator wall; 7: Sandwich calorimeter; 8: Beam monitor.

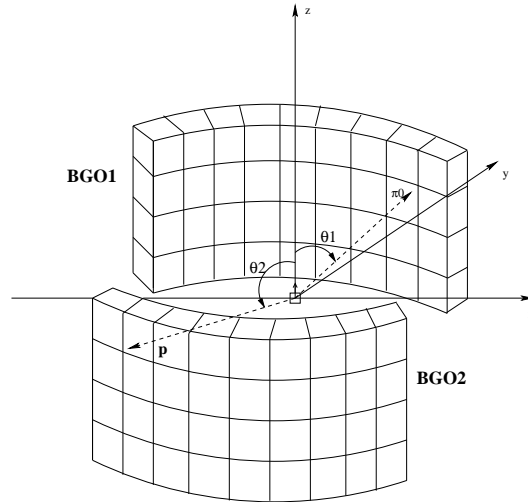


FIG. 11: A simplified model of the BGO calorimeter used for a test simulation of the detection of πN and NN pairs. The photon beam is along the axis z .

momentum and the reconstructed mass of the pion, $m_{\pi^0} = \sqrt{2E_{\gamma_1}E_{\gamma_2}(1 - \cos\theta_{\gamma_1\gamma_2})}$; the deviation of these quantities from 90° and 135 MeV, respectively, gives a rough idea on the accuracy of using the BGO calorimeter for reconstructing the events.

Note, in particular, that the measured total energy $E_{\pi^0} + E_p$ gives us an estimate of the binding effect for η in the nucleus. With the same aim we show in Fig. 16 a two-dimensional

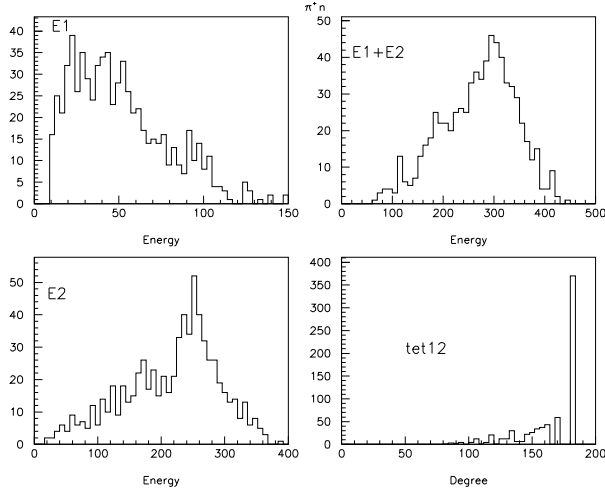


FIG. 12: Energy depositions and angular distribution of n and π^+ detected in the BGO calorimeter. Notation: $E1 = E_n$, $E2 = E_{\pi^+}$, $tet12 = \theta_{n\pi^+}$.

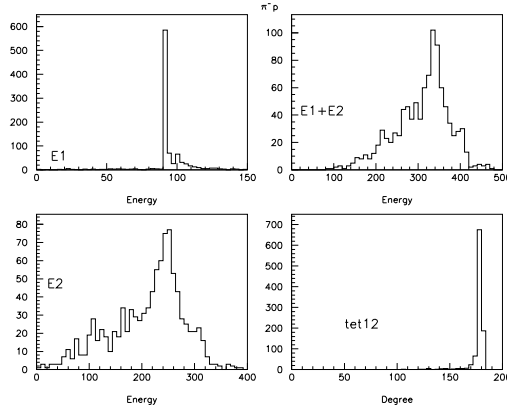


FIG. 13: Energy depositions and angular distribution of p and π^- detected in the BGO calorimeter. Notation: $E1 = E_p$, $E2 = E_{\pi^-}$, $tet12 = \theta_{p\pi^-}$.

angular distribution of energy depositions $dE/dz d\phi$ for photons, decay products of π^0 .

In Figure 17, shown are simulated distributions over the total energy deposited by πN pairs of different electric charges in the model BGO detector. Then all four decay channels of η -nuclei, i.e. π^+n , π^-p , π^0p and π^0n , are added with appropriated weights (1/3, 1/3, 1/6 and 1/6, respectively) to give a combined histogram shown in the bottom of Fig. 17.

This figure clearly shows that the calorimetric method of detection of the πN pairs is quite suitable only for the π^0p channel. Three other channels do not assure a full energy deposition and lead to large fluctuations. They rather give a broad background which though can be suppressed by veto detectors or alike. Note that there are also other contributions to the background, e.g. one from double-pion photoproduction off the nucleus. Moreover,

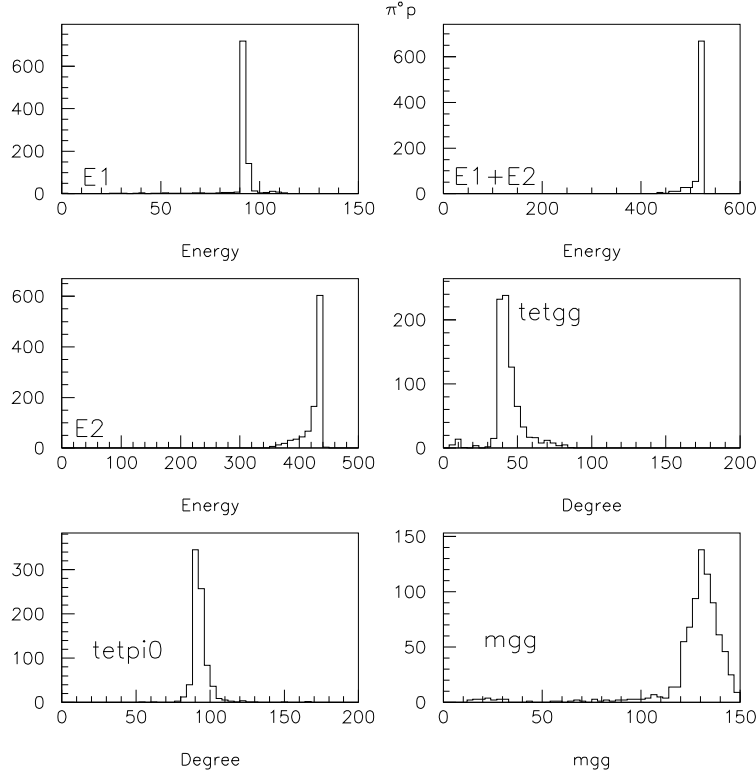


FIG. 14: Energy depositions and angular distribution of p and π^0 detected in the BGO calorimeter. Notation: $E1 = E_p$, $E2 = E_{\pi^0}$, $\text{tetgg} = \theta_{\gamma_1\gamma_2}$, tetpi0 is the reconstructed angle θ_{π^0} , and mgg is the reconstructed invariant mass $m_{\gamma_1\gamma_2}$.

energy losses in a bigger target will be larger.

From all these figures we conclude that among 4 charge states πN only the channel $\pi^0 p$ can be used for accurate measurements suitable for the purposes of the present experiment. The channel pp is suitable too, as can be inferred from Fig. 18. Thus, together with the forward-flying proton ($E_{p_1} \sim 250$ MeV), we choose the coincidence $(p_1, \gamma\gamma[\pi^0], p)$ as the trigger for the reaction (7), Fig. 6, where $\gamma\gamma[\pi^0]$ means two photons with the invariant mass of the neutral pion. The trigger for the reaction (8), Fig. 6, is the triple coincidence $(p_1, p_2 p_3)$ of the forward-flying proton with two protons in the BGO calorimeter. At last, the trigger for the reaction (9), Fig. 8, is the coincidence $(p_1, \gamma\gamma[\eta])$, where $\gamma\gamma[\eta]$ means two photons with the invariant mass of the η -meson; though, six-photon events from the $\eta \rightarrow 3\pi^0$ could also be recorded and then analyzed. Note that $\pi^0 p$ pairs produced through annihilation of slow η in the nucleus have a nearly isotropic distribution and have the opening angle $\theta_{\pi^0 p}$ close to 180° . In the case of the two-photon decay of slow η (or the two-proton decay of $S_{11}(1535)$ through $S_{11}^+(1535) + p \rightarrow p_2 + p_3$) the angular distribution of photons (protons) is again nearly isotropic and the opening angle $\theta_{\gamma_1\gamma_2}$ ($\theta_{p_2 p_3}$) is close to 180° .

The electronic trigger of the events in the $(p_1, \pi^0 p)$ channel will include simultaneous signals in the cylindrical wire chambers and in three BGO counters C_1, C_2, C_3 (see Fig. 19). The signals in the wire chambers show the path of the charged particle (the proton), with the C_1 BGO-counter giving the energy loss of the proton, ΔE_p . Signals in the C_2 and C_3 counters lying opposite to the C_1 counter indicate a detection of two photons from the π^0 decay. The total energy deposited in the BGO crystals plus the energy carried by the

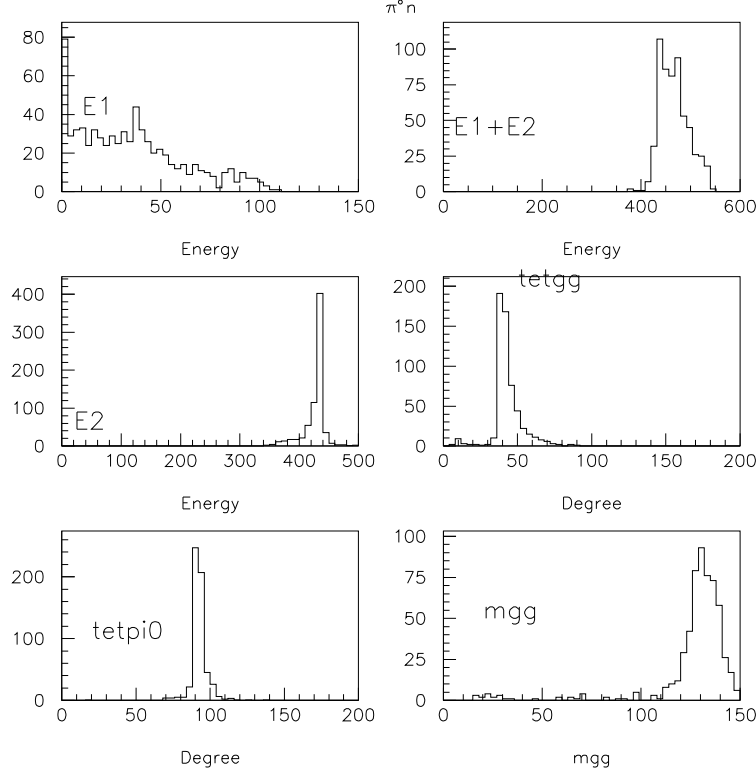


FIG. 15: Energy depositions and angular distribution of n and π^0 detected in the BGO calorimeter. Notation: $E1 = E_n$, $E2 = E_{\pi^0}$, $tetgg = \theta_{\gamma_1\gamma_2}$, $tetpi0$ is the reconstructed angle θ_{π^0} , and mgg is the reconstructed invariant mass $m_{\gamma_1\gamma_2}$.

forward-flying proton p_1 must match the initial photon energy E_γ up to, possibly, a small excitation energy of the rest of the nucleus.

C. Estimates of count rates

• The count rate of η -nuclei production through the coincidences $(p_1, \pi^0 p)$ at GRAAL can roughly be estimated as

$$Y(p_1, \pi^0 p) = \sigma_{(\eta A)} N_\gamma N_n \frac{\Delta\Omega_p}{4\pi} f_{\pi^0} f_{p_1} \text{Br}(\pi^0 p) \simeq 500 \frac{\text{events}}{\text{day}}, \quad (10)$$

where

$\sigma_{(\eta A)} \simeq 0.5 \mu\text{b}$ is the total cross section of η -nuclei photoproduction inside a nucleus in the reaction $\gamma + {}^{12}\text{C} \rightarrow p + {}^{11}_\eta\text{B}$ [30], in which only nuclear protons contribute to η production; an average over the energy interval of $E_\gamma = 700\text{--}1000$ MeV is assumed;

$N_\gamma \simeq 2 \cdot 10^5 \text{ s}^{-1}$ is the number of tagged photons over the energy interval 700–1000 MeV;

$N_n \simeq 7 \cdot 10^{23}$ is the number of nuclei ${}^{12}\text{C}$ in the target of the length 6 cm;

$\Omega_p \simeq 11$ rad is the solid angle covered by the BGO spectrometer where protons are detected;

$f_{\pi^0} \simeq 0.8$ is the efficiency of detecting $\gamma_1\gamma_2$ from the π^0 decay in the BGO spectrometer;

$f_{p_1} \simeq 0.7$ is a fraction of forward-flying protons generated in the process of η -nucleus formation and detected by the time-of-flight wall;

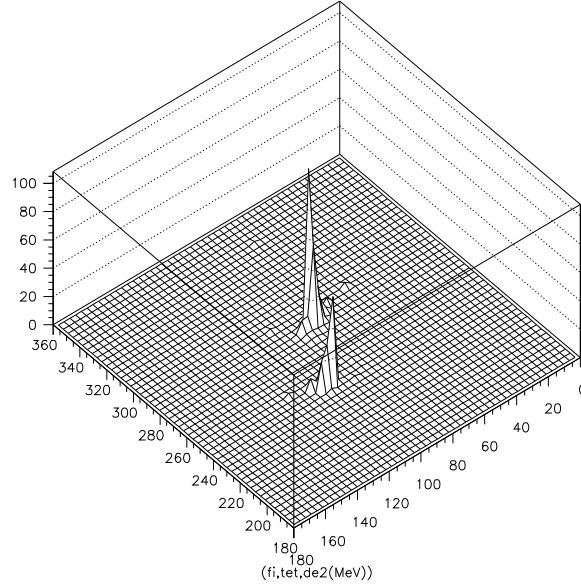


FIG. 16: The two-dimensional distribution of energy depositions over the polar and azimuthal angles, θ and ϕ , for two photons, decay products of π^0 flying from the target at $(90^\circ, 270^\circ)$ with the energy $E_{\pi^0} = 300$ MeV.

$\text{Br}(\pi^0 p) = \frac{1}{6}$ is the branching ratio to generate the channel $\pi^0 p$ in the process of annihilation of η inside the nucleus among four possible alternatives $\pi^0 p$, $\pi^+ n$, $\pi^- p$, $\pi^0 n$.

The count rate (10) is quite reasonable for observation because of a strong suppression of backgrounds due to multiple coincidences.

- The count rate of η -nuclei production through the coincidences $(p_1, p_2 p_3)$ at GRAAL can roughly be estimated as

$$Y(p_1, p_2 p_3) = \sigma(\eta A) N_\gamma N_n \left(\frac{\Delta\Omega_{p_2}}{4\pi} \right) f_{p_2 p_3} \text{Br}(pp) \simeq 120 \frac{\text{events}}{\text{day}}, \quad (11)$$

where

$f_{p_2 p_3} \simeq 0.8$ is an efficiency to detect the correlated proton pair from the subprocess $S_{11}^+(1535) + p \rightarrow p_2 p_3$;

$\text{Br}(pp) \simeq 0.1 \cdot \frac{1}{4}$ is the branching ratio of the η -nucleus decay through the two-nucleon absorption (about 10% of NN pairs in comparison with 90% of ηN decays through the πN channel [15]) times the fraction 1/4 to have $NN = pp$.

- The count rate of slow- η production through the coincidences $(p_1, \gamma_1 \gamma_2[\eta])$ at GRAAL can roughly be estimated as

$$Y(p_1, \eta) = \sigma_t(\eta) N_\gamma N_n f_\eta f_{p_1} \simeq 75000 \frac{\text{events}}{\text{day}}, \quad (12)$$

where

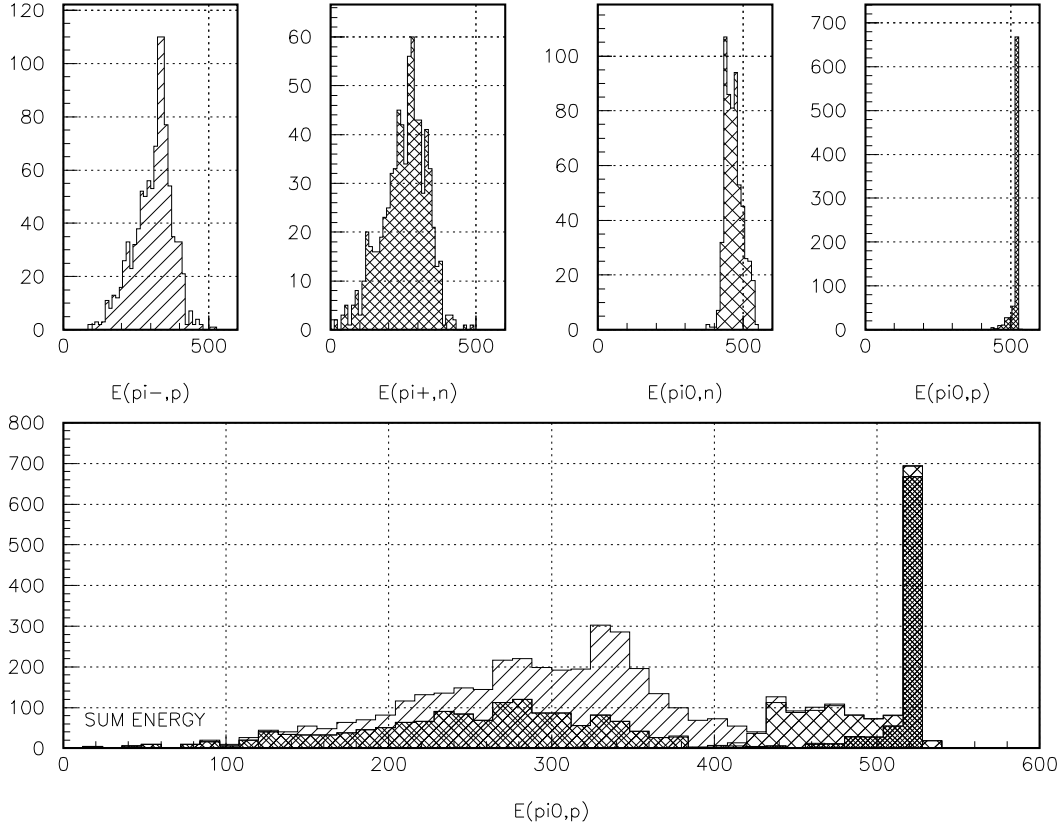


FIG. 17: Top: energy depositions of πN pairs with different charges in the BGO calorimeter. Bottom: a combined (with appropriate weights 1/3, 1/3, 1/6, 1/6) distribution which thus gives an idea of a background.

$\sigma_t(\eta) \simeq 25\mu\text{b}$ [31] is the total cross section of η photoproduction off protons in the nucleus ^{12}C with the kinetic energy of η below 70 MeV; this condition corresponds to the backward-angle production of η in the subprocess $\gamma p \rightarrow \eta p$; an average over the energy interval of $E_\gamma = 700\text{--}1000$ MeV is assumed;

$f_\eta \simeq 0.8$ is the efficiency of detecting $\gamma_1\gamma_2$ from the η decay by the BGO spectrometer;

$f_{p_1} \simeq 0.3$ is a fraction of forward-flying protons generated in the process of slow- η production and detected by the time-of-flight wall.

Note that the count rate of the $(p_1, \gamma_1\gamma_2[\eta])$ events coming from radiative decays $\eta \rightarrow \gamma_1\gamma_2$ of the bound η is expected to be $\sim 10^4$ times less than Eq. (10) gives, thus being of order 0.1 events/day and too small to be detected.

III. SUMMARY OF AIMS AND PERSPECTIVES

In conclusion, studies of η -mesic nuclei lie at the interception of the nuclear physics and the physics of hadrons and they promise to bring a new information important for both the

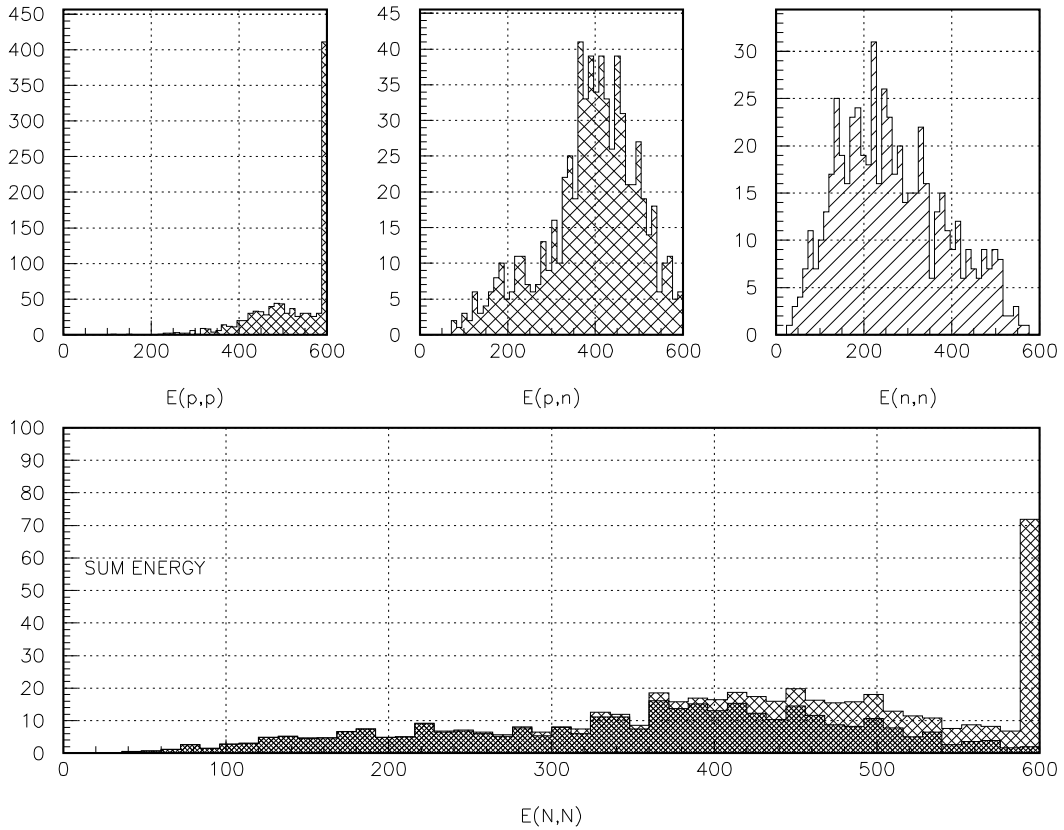


FIG. 18: Top: energy depositions of NN pairs with different charges in the BGO calorimeter. Bottom: a combined distribution (with appropriate weights $1/3, 1/3, 1/6, 1/6$); it gives an idea of background.

fields. Such studies are quite feasible at electron accelerators with bremsstrahlung beams. Tagged photon beams can also be used. The main aims and perspectives of the proposed experiment can be summarized as follows:

- Generally, we expect to bring a novel experimental information on behavior of the η -meson in the nuclear matter. Specifically, we hope to measure energy levels E_η and widths Γ_η of the bound η -nucleus systems and compare them with modern calculations. It is worth to say that theoretical values for E_η and Γ_η strongly depend on the potential $V_{\eta N}$ and the scattering amplitude $f_{\eta N}$ assumed for the elementary ηN interaction and on the dynamics of dressing η and $S_{11}(1535)$ in the nuclear matter [10–15].
- We will measure separately two different channels, πN and NN , of η -nucleus decays. This will provide a valuable test for dynamics of the $S_{11}(1535)$ resonance in the nuclear matter.
- In parallel, we will study near-threshold production of η -mesons which is expected to have a strong energy dependence due to attractive forces between η and the nucleus.

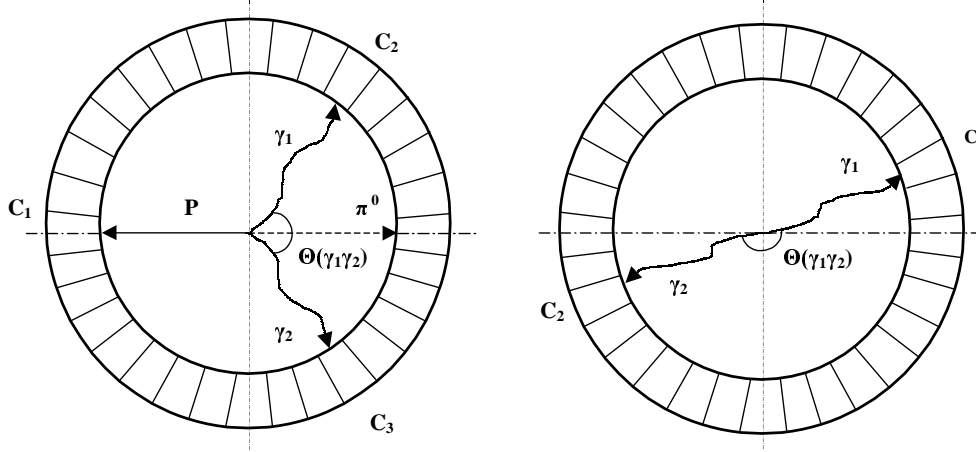


FIG. 19: The topography of detected events in the BGO calorimeter.

The data on this energy dependence provide a further useful input for constraining existing theoretical models for ηN and ηA interaction.

- In a perspective, studies of η -nuclei can open a way towards wider investigations of (ρ, ω, φ) -nuclear systems which are presently discussed in the literature [32].

Acknowledgments

This work was supported by the Russian Foundation for Basic Research, grant #02-02-16519.

-
- [1] R.S. Bhalerao and L.C. Liu, Phys. Rev. Lett. **54**, 865 (1985).
[2] R.A. Arndt, I.I. Strakovsky and R.L. Workman, Phys. Rev. C **53**, 430 (1996).
[3] B. Krusche et al., Phys. Rev. Lett. **74**, 3736 (1995).
[4] M. Roebig-Landau et al., Phys. Lett. B **373**, 45 (1996).
[5] G.-Y. Chen, S.S. Kamalov, S.N. Yang, D. Drechsel and L. Tiator, nucl-th/0210013.
[6] R.A. Arndt, W.J. Briscoe, I.I. Strakovsky and R.L. Workman, Phys. Rev. C **66**, 055213 (2002).
[7] A.M. Green and S. Wycech, Phys. Rev. C **55**, R2167 (1997).
[8] M. Batinic et al., nucl-th/9703023.
[9] N. Kaiser, T. Waas and W. Weise, Nucl. Phys. A **612**, 297 (1997).
[10] Q. Haider and L. Liu, Phys. Lett. B **172**, 257 (1986); Erratum: *ibid.* **174**, 465 (1986);
L.C. Liu and Q. Haider, Phys. Rev. C **34**, 1845 (1986).
[11] J. Kulpa, S. Wycech and A.M. Green, nucl-th/9807020.
[12] Q. Haider and L.C. Liu, Phys. Rev. C **66**, 045208 (2002).
[13] C. Garcia-Recio, J. Nieves, T. Inoue and E. Oset, Phys. Lett. B **550**, 47 (2002).
[14] D. Jido, H. Nagahiro and S. Hirenzaki, Phys. Rev. C **66**, 045202 (2002).
[15] H.C. Chiang, E. Oset and L.C. Liu, Phys. Rev. C **44**, 738 (1991).
[16] J.C. Peng, AIP Conference Proceedings **133**, 255 (1985).
[17] S.A. Rakityansky et al., Phys. Rev. C **53**, R2043 (1996).

- [18] J. Berger et al., Phys. Rev. Lett. **61**, 919 (1988).
- [19] N. Willis et al., Phys. Lett. B **406**, 14 (1997).
- [20] B. Mayer et al., Phys. Rev. C **53**, 2068 (1996).
- [21] V. Hejny et al., Eur. Phys. J. A **13**, 493 (2002).
- [22] R.E. Chrien et al., Phys. Rev. Lett. **60**, 2595 (1988).
- [23] B.J. Lieb and L.C. Liu, "Progress at LAMPF", Report LA-11670-PR (1988).
- [24] G.A. Sokol et al., Fizika B **8**, 81 (1998); nucl-ex/0011005.
- [25] A.I. L'vov, nucl-th/9810054.
- [26] G.A. Sokol et al., nucl-ex/0011005.
- [27] V.P. Pavlyuchenko. Voprosy Atomnoi Nauki i Tekhniki, seria Tekhnika Fizicheskogo Eksperimenta, **1/13**, 39 (1982).
- [28] F. Ghio et al., Nucl. Instr. Meth. A **404**, 71 (1998).
- [29] V. Kouznetsov et al., Nucl. Instr. Meth. A **487**, 128 (2002).
- [30] A.I. Lebedev and V.A. Tryasuchev, Yad. Fiz. **58**, 642 (1995).
- [31] B.Krusche, Acta Physica Polonica B **27**, 3147 (1996).
- [32] K. Tsushima, in Proc. XIV Intern. Seminar on High Energy Physics Problems, Dubna, 17-22 Aug 1998, Eds. E.M. Baldin and V.V. Burov, Dubna 2000, p. 120.